

observations are marred by a large amount of dust, making the determination of the galaxy's axial ratios somewhat unreliable, still these arguments have received considerable support by the ability of the triaxial-bulge model to explain the gross departures from the axially-symmetric rotational velocity field observed in this galaxy.

In conclusion, we have shown that purely geometrical evidence shows that bulges are triaxial, a conclusion also supported by dynamical evidence, which re-establishes the similarity between bulges and elliptical galaxies.

Acknowledgement

W.W.Z. acknowledges the support of this project by the Austrian *Fonds zur Förderung der wissenschaftlichen Forschung* (project P 5529).

References

Aarseth, S.J. and Binney, J.J., 1978. *Mon. Not. Roy. Astr. Soc.*, **185**, 227.
 Bertola, F., 1972. in *Proc. 15th Meeting of the Ital. Astron. Soc.*
 Bertola, F. and Capaccioli, M., 1975. *Astrophys. J.*, **200**, 439.
 Bertola, F. and Galletta, G., 1979. *Astron. Astrophys.*, **77**, 363.
 Bertola, F., Bettoni, D., Danziger, J., Sadler, E.M. and de Zeeuw, T., 1988, in preparation.
 Boronson, T., 1981. *Astroph. J. Suppl. Ser.*, **46**, 177.
 Capaccioli, M. and Vietri, M., 1988. *Mon. Not. Roy. Astr. Soc.*, in press.
 Davies, R.L., 1987. in *Structure and Dynamics of Elliptical Galaxies*, I.A.U. Symp. 127, ed. T. de Zeeuw (Dordrecht:Reidel) p. 63.
 Davies, R.L. and Birkinshaw, M., 1986. *Astrophys. J.*, **303**, L45.
 Gamaleldin, A.I. and Issa, I.A., 1983. *Astron. Nachr.*, **304**, 21.

Gerhard, O. and Vietri, M., 1986. *Mon. Not. Roy. Astr. Soc.*, **223**, 377.
 Gerhard, O. and Vietri, M., 1987, in *Structure and Dynamics of Elliptical Galaxies*, I.A.U. Symp. 127, ed. T. de Zeeuw (Dordrecht:Reidel) p. 399.
 Illingworth, G., 1977. *Astrophys. J.*, **204**, 73.
 Kormendy, J., 1982. *Astrophys. J.*, **257**, 75.
 Lake, G., 1987, in *Structure and Dynamics of Elliptical Galaxies*, I.A.U. Symp. 127, ed. T. de Zeeuw (Reidel) p. 331.
 Lauberts, A., 1982. *The ESO/Uppsala Survey of the ESO (B) Atlas* (ESO).
 Lindblad, B., 1956. *Stockholm Obs. Ann.*, **19**, No. 2.
 Schwarzschild, M., 1979. *Astrophys. J.*, **232**, 236.
 Stark, A.A., 1977. *Astrophys. J.*, **213**, 368.
 White, S., 1987, in *Structure and Dynamics of Elliptical Galaxies*, I.A.U. Symp. 127, ed. T. de Zeeuw (Dordrecht:Reidel) p. 339.
 Zaritsky, D. and Lo, K.Y., 1986. *Astrophys. J.*, **303**, 66.

Simulations of High Redshift Galaxies and Observations with the Hubble Space Telescope

T. J.-L. COURVOISIER,* ST-ECF, and A. LAUBERTS, ESO

The high angular resolution of the Hubble Space Telescope (HST) will allow the observations of the structure of small but extended objects. Prime candidates for this type of research are galaxies at moderate or high redshifts. These galaxies are approximately 1" in diameter and will contain many resolution elements of the space telescope. The exact resolution will depend on the wavelength of the observation and on the mode in which the observations will be made, the highest resolution being obtained with the faint object camera in the f/288 mode. Since most imaging modes will provide a resolution better than ~0".1, galaxies at large redshift will cover more than ~100 resolution elements. The Wide Field Camera (WFC) with a field of view of 3' x 3' is well suited for statistical studies of the properties of field galaxies, although its spatial resolution will be limited by the pixel size to .1". The number of galaxies that can usefully be studied in each exposure naturally depends on the depth of the exposure, at V ~ 25 it is expected to be of the order of 100 galaxies.

In order to assess the potential of HST-WFC for the observation of random fields, we conducted a programme of simulations of galaxies and their "ob-

servations" with the WFC simulator developed at the ST-ECF (Rosa and Baade 1986). The starting point of our simulations was a set of 14 nearby galaxies of all Hubble types observed with the ESO Schmidt telescope, in the colours B and R, digitized and calibrated. U and V images were computed using a linear combination of the B and R images with coefficients based on a sample of multi-aperture photoelectric UBV photometry. We shifted the galaxies to different distances, constructed a field of galaxies (3' x 3') and "observed" this field with the HST simulator.

Individual Galaxies

We shifted the galaxies to different distances, scaling the angles as appropriate for a Friedmann cosmology with $q^0=0$. The K-correction which needs to be applied to take the redshift into account was applied locally, pixel by pixel. This was done by calculating the colour of the individual pixels (the images were all shifted so that the centroid of the galaxy corresponded on all the frames taken for each galaxy). This colour was compared with the integrated colour of galaxies for which K-corrections are available (Coleman et al. 1980), and the K-correction of the standard galaxy with colour closest to the pixel colour was applied for the desired red-

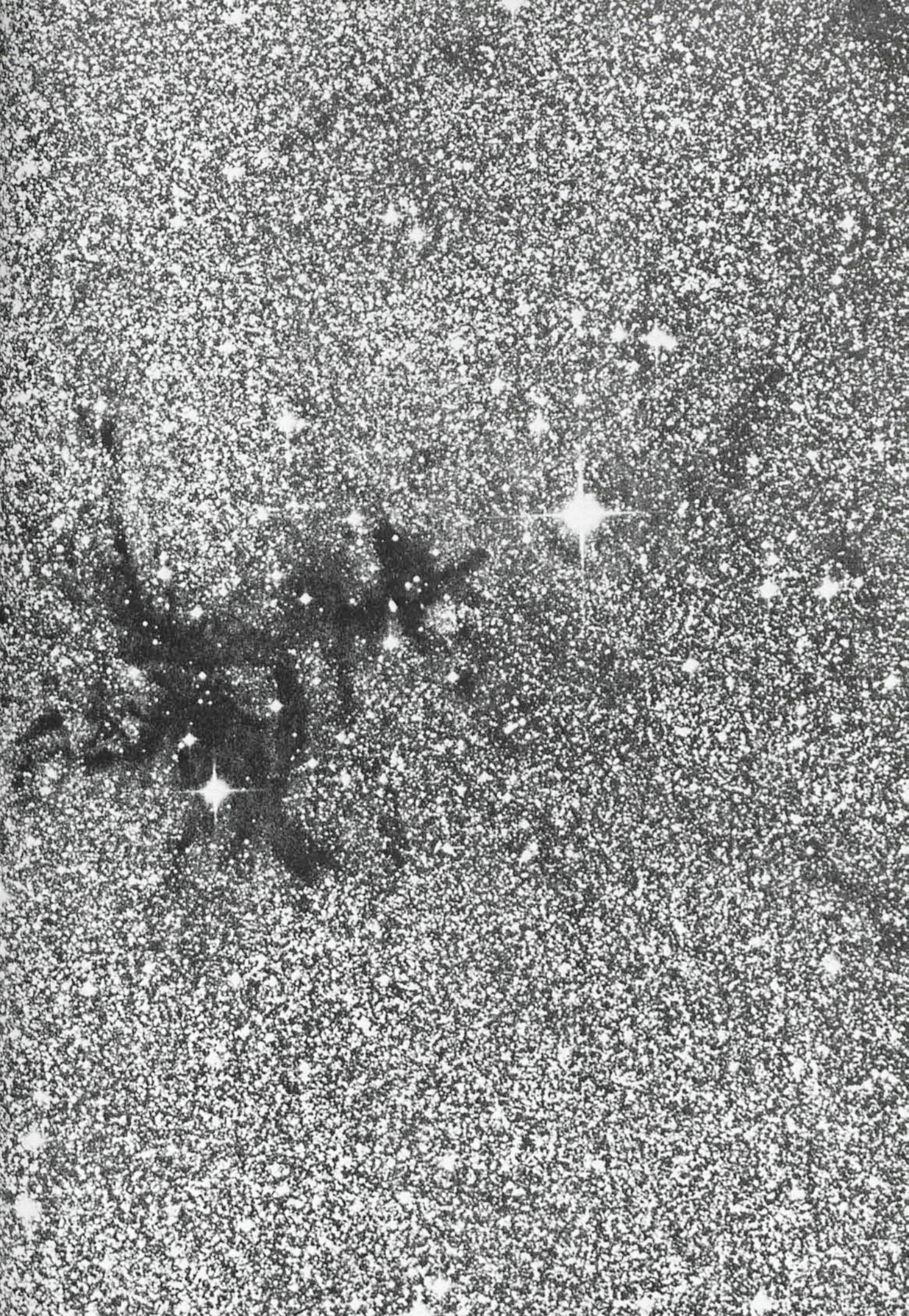
shift. This procedure allows to correct the individual features of a galaxy, and hence to study the apparent evolution of the galaxy with redshift. No intrinsic evolution has been taken into account for the time being.

Our scheme to apply K-corrections has several shortcomings: Ideally the K-correction should be calculated for the individual components of a galaxy and applied to each component separately, the components being identified by their colour and location in the galaxy. In addition, reddening by dust in the galaxy modifies the spectrum of individual features and therefore the K-corrections that ought to be applied. Our procedure identifies the different
(continued on p. 30)

The centerfold shows a highly structured molecular cloud which is located in the southern constellation Norma, a region with many dark clouds. The cloud is clearly divided in two parts, a large irregular "head" and a long, thin "tail". The almost complete extinction of the rich background star fields in the Milky Way indicates that the clouds are very dense. Star formation is taking place at various points in the cloud, and two Herbig-Haro objects, HH 56 and HH 57, are found in the head. The energy source of HH 57 erupted just a few years ago in a so-called FU Orionis outburst, and is now a bright infrared source. This is one of the first star-forming

* Affiliated to the Astrophysics Division of the Space Science Department of ESA.

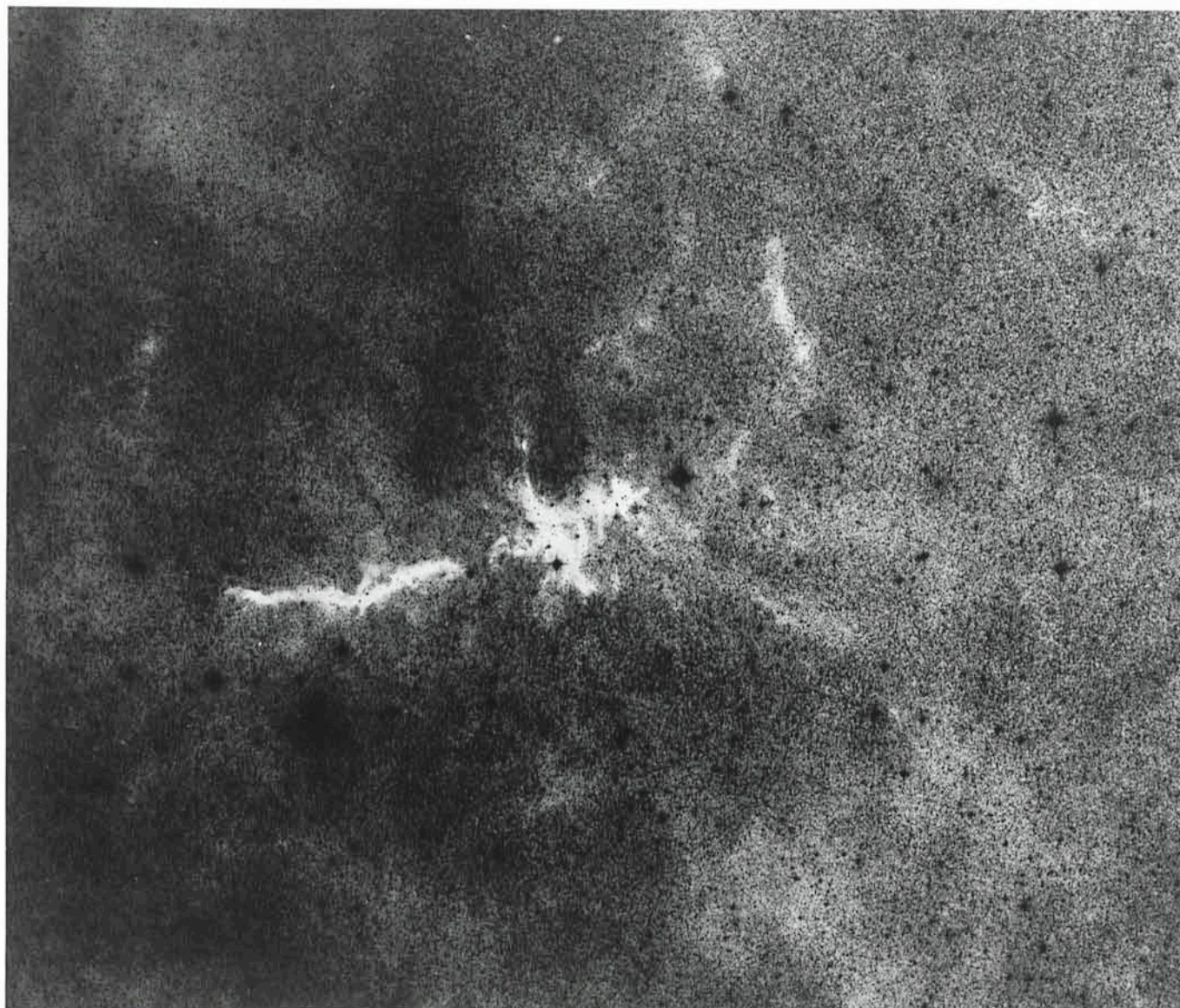




regions observed with the new SEST millimetre-wave telescope at La Silla. The observations revealed the presence of a large bipolar outflow, formed by energetic stellar winds from energy sources of the Herbig-Haro objects. All young stars are believed to pass through early phases with strong stellar winds, which will clear away the ambient material left over from the birth of the stars. To reveal the details of this highly structured cloud, the original plate was subjected to a combination of unsharp masking and diffuse-light amplification.

The smaller photo on this page shows the surroundings of the cloud. Here the reproduction is negative to bring out the nearby structures, which are somewhat less dense.

From a deep, red-sensitive ESO Schmidt plate (150 min; IIIa-F + RG630). Observers: H.-E. Schuster and G. Pizarro. Text by B. Reipurth; photographic work by C. Madsen.



(continued from p. 27)

components of a galaxy on their colour only and approximates the K-correction by assuming that the typical galaxies for which K-corrections are given in the literature correspond to these single components.

Since our original images had been well exposed, the signal-to-noise ratio is good in all the galaxies and we do not expect that random colour fluctuations have had any impact on the resulting frames. This can be seen in that the K-corrected images look as smooth as the original images (Fig. 1, 2 and 3). Where the signal to noise per pixel did not allow to determine a colour (sky), no K-correction was applied. In the outer parts of the galaxies, where the galaxy signal is

between 10% and 50% of the sky level, the colour of the pixels used in the K-correction procedure was calculated using the average colour of the complete galaxy.

Figure 1 gives the late type galaxy NGC 1365 at a redshift of 0.0054 in the U, B, V and R filters. Figures 2 and 3 give the same galaxy in the same colours but with the K-correction applied as described above for a redshift of $z=0.5$ and $z=1$. It is immediately apparent that the structure of the galaxy has changed in that the arms become more prominent in the $z=0.5$ and $z=1$ U images than in the original image, to the point that the brightest parts of the galaxy are to be found in the arms and

not in the nucleus as is the case at low redshift. In the red image, the bar and bulge disappear at $z=1$, leaving a structure dominated by the nucleus and the arms.

Elliptical galaxies, having no azimuthal colour structure at $z=0$ keep this symmetry also at high redshift. Therefore, early type galaxies show less morphological changes with redshift than late type galaxies. In general, the bar of barred galaxies decreased in relative intensity in U and B with increasing redshift. This tendency is less pronounced in V and R.

In summary, the galaxies at high redshift appear to be of later type than at low redshift. This trend is more pro-

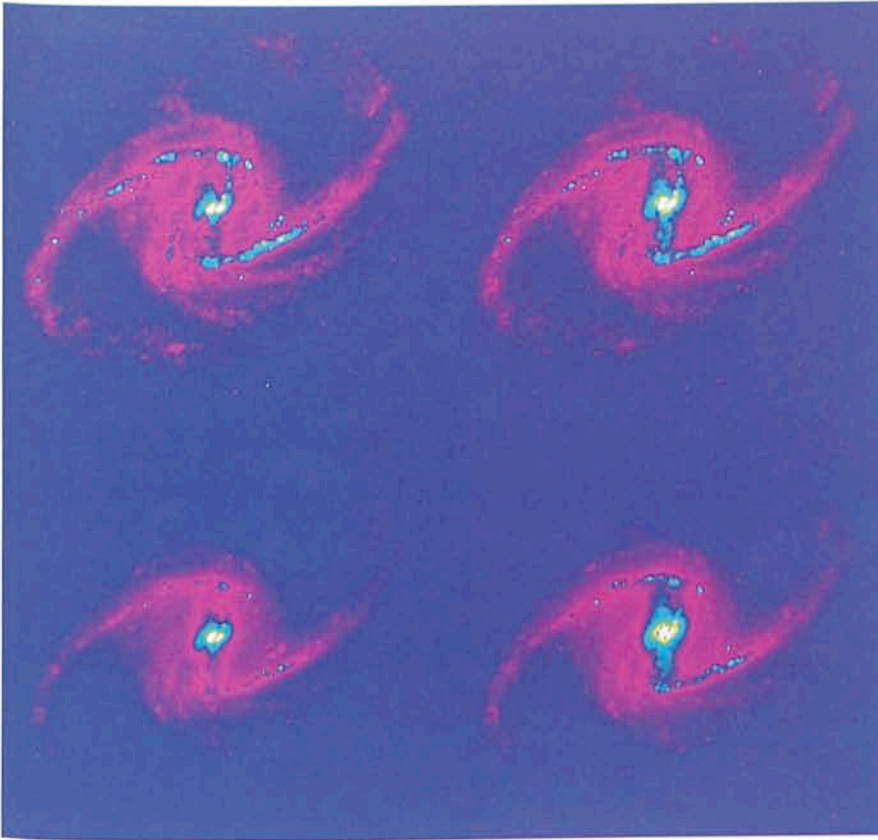


Figure 1: The Galaxy NGC 1365 at the redshift $z=0.0054$. The upper right panel gives the B image, upper left panel the U image, the lower left panel the V image and the lower right panel the R image.



Figure 2: Same galaxy and colours as Figure 1 but at a redshift $z=0.5$. The image was shifted as described in the text.

nounced for already late type galaxies and for U and B images than for early type galaxies and V and R images. The Hubble classification of galaxies also doesn't match the high redshift galaxies as well as it matches the low z observed galaxies.

Field of Galaxies

The galaxies we used to study the effect of redshift on the morphological type were also used to construct a $3' \times 3'$ field of the sky. This was done using a random distribution of galaxies in 3 dimensions, characterized by a mean galaxy surface density of ~ 800 galaxies per $5' \times 5'$ and no clustering. The galaxy types were matched with our sample galaxies, the K-corrections applied as described above and the galaxies randomly flipped and rotated. The resulting frame is given in Figure 4. The resolution of the display used to generate Figure 4 is limited to 512×512 pixels, so that Figure 4 has only $\frac{1}{4}$ of the WFC resolution.

A $51''.2 \times 51''.2$ part of this frame (lower left of Figure 4) was then "observed" with the WFC HST simulator of the ST-ECF. The effects of seeing were approximated by the re-binning of the frame to the pixel size of the WFC ($0''.1$) as this is the dominant effect of the instrument resolution. Several noise effects were taken into account in the simulations: photon noise, preflash electrons, deferred charge and read out noise. The signal was calculated using the magnitude of the galaxies at the corresponding redshift, the effective surface of HST, the filter transmission and the detector quantum efficiency. The integration times were chosen to correspond to realistic exposures. The images were expressed in ADU counts and a bias was added to the images.

Several effects of real images were not simulated, these include the presence of point sources in the field (expected to amount to 10% of the sources at high galactic latitude), cosmic rays and the lack of uniformity of the detector sensitivity (flat fields).

Figure 5 gives the resulting V-image following a 2,500-second integration.

Galaxies down to V mag of ~ 24 integrated magnitude can still be seen. The brightest galaxy has an integrated V magnitude of 19.6. The limiting surface brightness for which useful morphological information can still be obtained will depend on the procedure used to analyse the images. The nucleus of an Sc galaxy at $z=0.98$ can still be seen on the image. More detailed analysis of the image will be performed by different groups using several algorithms and software in order to test the analysis

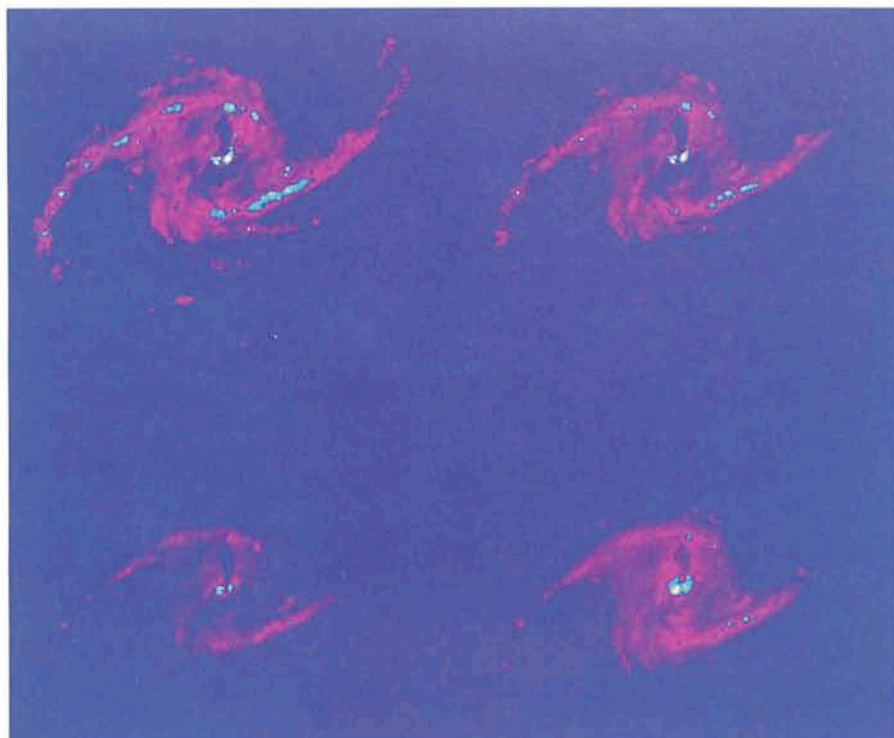


Figure 3: Same galaxy and colours as Figures 1 and 2 but at $z=1$.

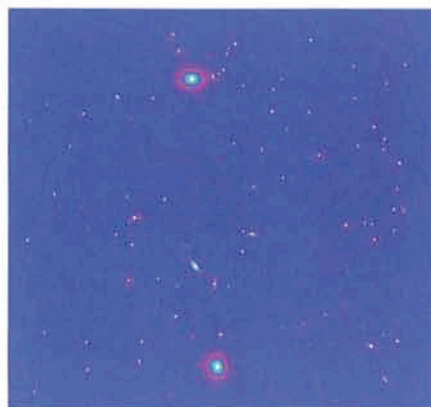


Figure 4: Simulated field of galaxies $3' \times 3'$. The galaxy distribution is a 3-D random distribution without clustering.

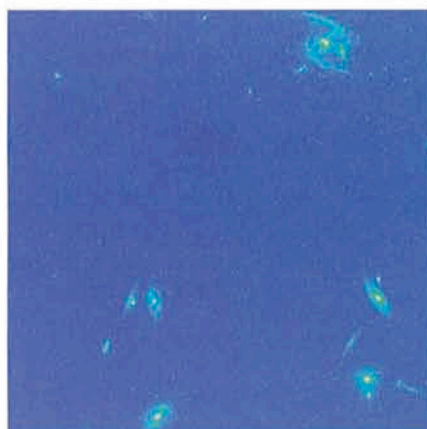


Figure 5: Simulated "observation" of the 51.2×51.2 lower left part of Figure 4 with the WFC of HST. The image is in a wide band filter approximating the V band, the exposure time of 2,500 s.

methods and show to which extent the information content of the image can be recovered.

Figure 6 gives the resulting B image after a 5,000-s integration. On this image, only the brightest features can still be distinguished. This shows the great difficulty to obtain colour information using U and B filters for extended objects with the WFC. In this wavelength domain, the faint object camera is expected to be more sensitive. Its smaller field of view will however reduce the sample of objects available in random fields.

We thank P. Vettolani for providing us with one of his simulations of the location, redshift and magnitudes of a random field of galaxies.

References

- Rosa and Baade 1986, *The Messenger* **45**.
 Coleman, Wu and Weedman, 1980, *Ap. J. Supp.* **43**, 393.

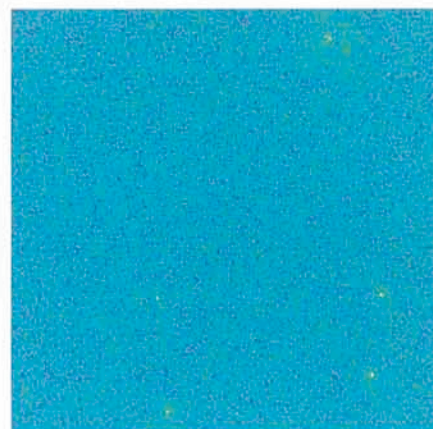


Figure 6: Same as Figure 5 but through a filter approximating the blue band and with an exposure time of 5,000 s.

List of ESO Preprints

(March–May 1988)

573. F. Matteucci and G. Vettolani: Chemical Abundances in Galaxy Clusters: a Theoretical Approach. *Astronomy and Astrophysics*.
 574. A. Iovino, J. Melnick and P. Shaver: The Clustering of HII Galaxies. *Astrophysical Journal*, Letters.
 575. H.-M. Adorf and E.J.A. Meurs: Supervised and Unsupervised Classification – The Case of IRAS Point Sources. F. Murtagh: Multivariate Analysis Methods: Background and Example.

Papers presented at the Bad Honnef meeting on "Large Scale Structures in the Universe – Observational and Analytical Methods". December 1987. In press, Springer-Verlag.

576. G. Meylan: On the Individual Masses of Globular Clusters in the Magellanic Clouds: NGC 1835. *The Astrophysical Journal*.
 577. F. Verbunt and G. Meylan: Mass Seggregation and Formation of X-ray Clusters. *Astronomy and Astrophysics*.
 578. R. Arsenault and S. D'Odorico: Medium Resolution Spectroscopy of the Supernova 1986 O in the Spiral Galaxy NGC 2227. *Astronomy and Astrophysics*.
 579. M. Pierre, P.A. Shaver and A. Iovino: Void Structure in the Lyman alpha

Forest. *Astronomy and Astrophysics*, Letter.

580. F. Matteucci and A. Tornambè: Theoretical Supernova Rates in the Galaxy and M31. *Astronomy and Astrophysics*.
 581. M.H. Ulrich and T.J.-L. Courvoisier: Short and Long Term Variations of the Ultraviolet Spectrum of 3C 273. *Astronomy and Astrophysics*.
 582. G. Contopoulos: Qualitative Characteristics of Dynamical Systems. In press in: A. Roy, "Long Term Behaviour of Natural and Artificial N-Body Systems", Reidel.
 583. G. Contopoulos: Critical Cases of 3-Dimensional Systems. *Celestial Mechanics*.